Supplementary Information

Dominant {100} Facet Selectivity for Enhanced Photocatalytic Activity of NaNbO₃ in NaNbO₃/CdS Core/Shell Heterostructures

Sandeep Kumar,[a,d] R. Parthasarathy,[a] Aadesh P. Singh,[b,c] Björn Wickman,[c] Meganathan Thirumal,[d] and Ashok K. Ganguli[a,e*]

[a]Department of Chemistry, Indian Institute of Technology Delhi, New Delhi-110016

[b]Department of Physics, Indian Institute of Technology Delhi, New Delhi-110016

[c]Division of Chemical Physics, Department of Physics, Chalmers University of Technology, SE-412 96 Gothenburg, Sweden

[d]Department of Chemistry, University of Delhi, Delhi 110007, India

[e]Institute of Nano Science & Technology, Mohali, Punjab-160062, India

Powder X-ray diffraction (PXRD) patterns of NaNbO₃/CdS core/shell heterostructures

Powder XRD analysis of both c-NaNbO₃/CdS and o-NaNbO₃/CdS core/shell heterostructuresproviding information regarding the phase composition,purity, and crystallinity of the synthesized materials is shown in Figure S1 (a and b). The qualitative analysis of the XRD patterns of c-NaNbO₃/CdS core/shell heterostructures (shown in Figure S1a) indicates that all the diffraction peaks of c-NaNbO₃ correlate closely with the documented cubic phase of NaNbO₃ (JCPDS card no. 191221), with some additional peaks are undisputedly indexed to (111) and (220) crystallographic planes of cubic CdS (JCPDS card no. 890440), respectively.In the same approach XRD patterns of o-NaNbO₃/CdS core/shell heterostructures (shown in Figure S1b) indicates that all the diffraction peaks of o-NaNbO₃ correlate closely with the documented orthorhombic phase of o-NaNbO₃ (JCPDS card no.898957) and additional peaks are indicates presence of cubic CdS (JCPDS card no.

890440). The XRD patterns undoubtedly reveal the core/shell heterojunction formation and presence of both materials.
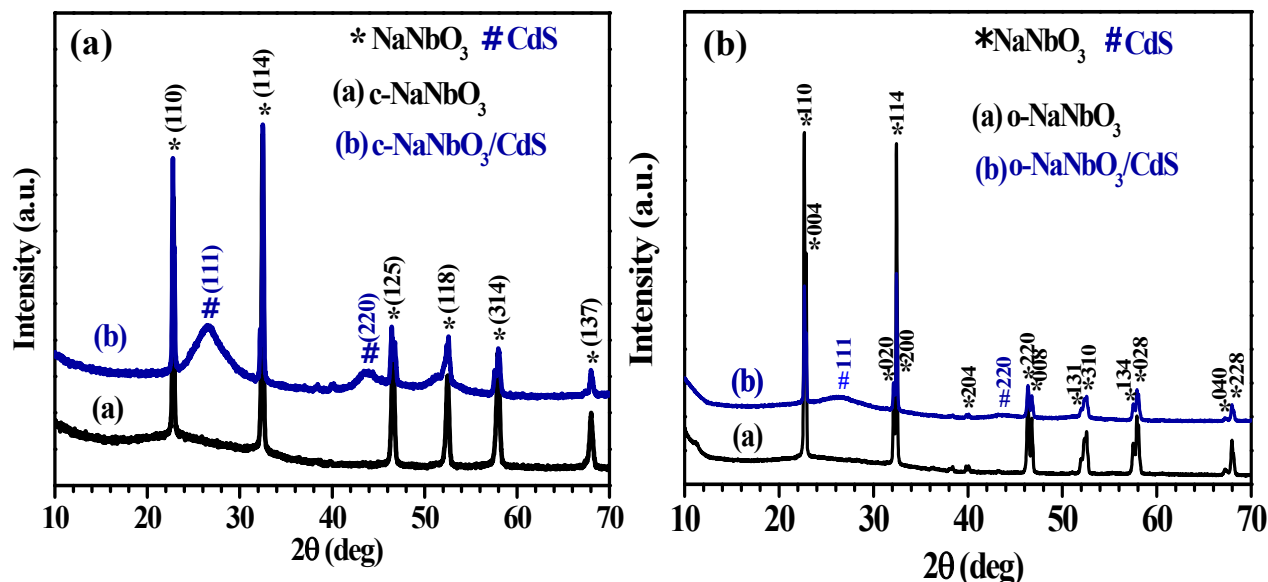
Figure S1.PXRD of (a) c-NaNbO$_3$/CdS cube and (b) o-NaNbO$_3$/CdS cuboctahedron core/shell respectively.

## Dynamic Light Scattering (DLS) of bare NaNbO$_3$ crystals

The size of NaNbO$_3$ crystals were also determined by dynamic light scattering (DLS) measurements by using Malvern Zetasizer Nano ZS-90 instrument (Malvern Instruments) shown in Figure S2. DLS measurement gives the particle size distribution in solution and recorded sizes of NaNbO$_3$ crystals are slightly higher than those obtained from TEM measurement because DLS captures the hydrodynamic diameter of dispersed materials.[1,2] Comparative size measure values are given below in Table S1.

Table S1:

Description	*Z-av (d. nm) (DLS)	Ave. Size (nm) (TEM)	**PDI
c-NaNbO$_3$	1880 ± 46	1722 ± 20	0.301
o-NaNbO$_3$	4879 ± 99	4815 ± 11	0.56
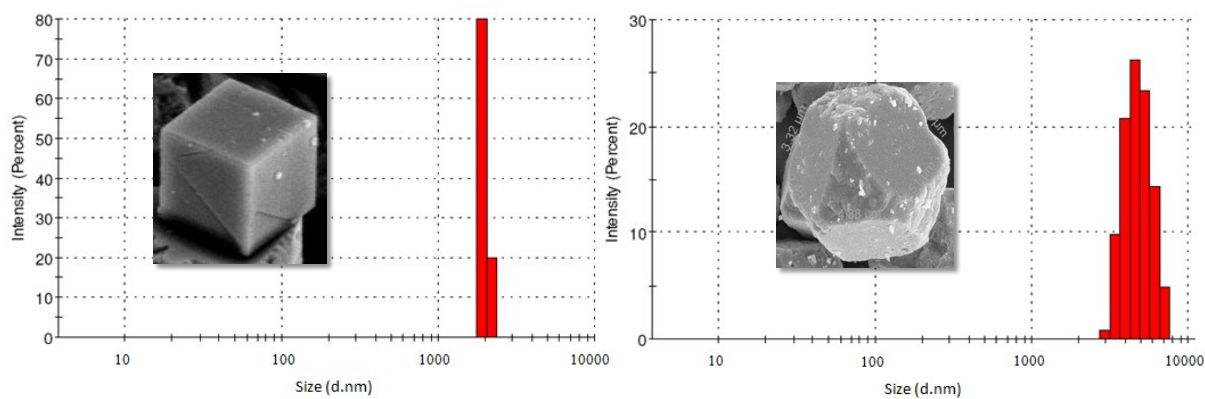
Figure S2. DLS size distribution image of (a) c-NaNbO$_3$ cube and (b) o-NaNbO$_3$ cuboctahedron respectively.

Lower field emission scanning electron microscope (FESEM) magnified image to determine the particle size and shape of bare NaNbO$_3$ crystals.
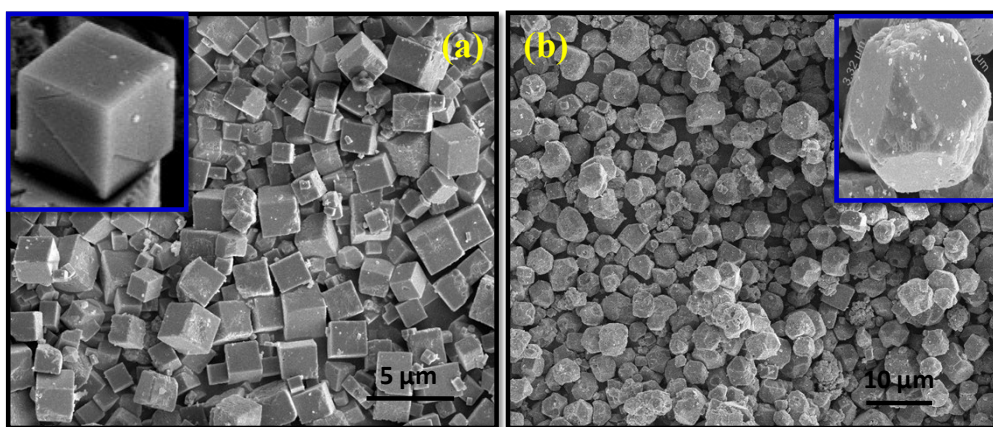

Figure S3. SEM size and shape distribution image of (a) c-NaNbO$_3$ cube and (b) o-NaNbO$_3$ cuboctahedron respectively.

Field Emission Scanning Electron microscopy (FESEM) images of NaNbO₃/CdS core/shell heterostructures

FESEM-EDS elemental mapping analysis was done to unravel the elemental composition and the amount of distribution of elements present in $NaNbO_3/CdS$ cube and cuboctahedron core/shell heterostructures as shown in Figure S4 (a &b) Mapping analysis brought out the coexistence of Na, Nb, O, Cd, and S elements in the heterostructures. Noticeably, the distribution of shell elements is homogeneous and uniform over cube and cuboctahedron core materials.
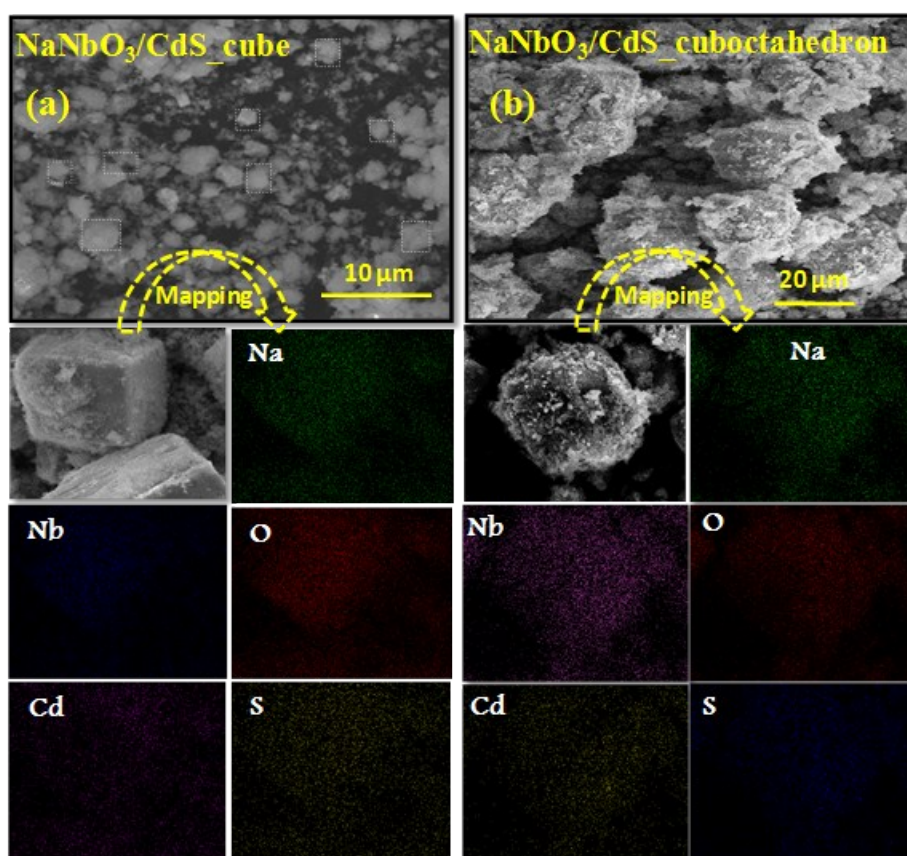

Figure S4. FE-SEM image along with elemental mapping of (a) c-$NaNbO_3/CdS$ cube and (b) o-$NaNbO_3/CdS$ cuboctahedron core/shell respectively.
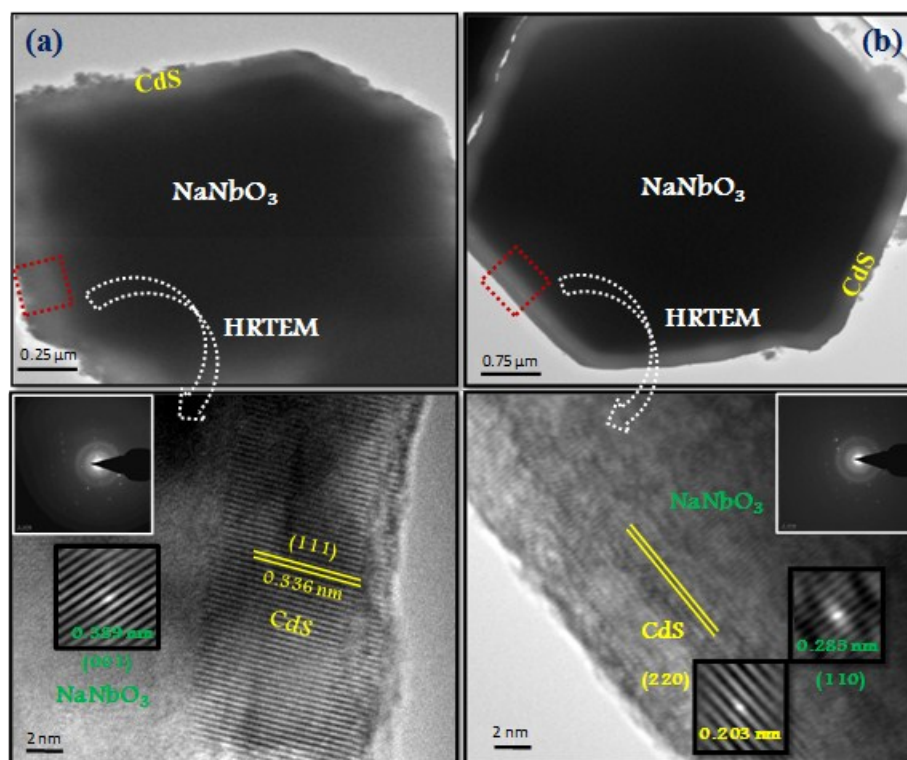
Figure S5. TEM and HRTEM image along with SEAD of (a) c-NaNbO$_3$/CdS cube and (b) o-NaNbO$_3$/CdS cuboctahedron core/shell respectively.
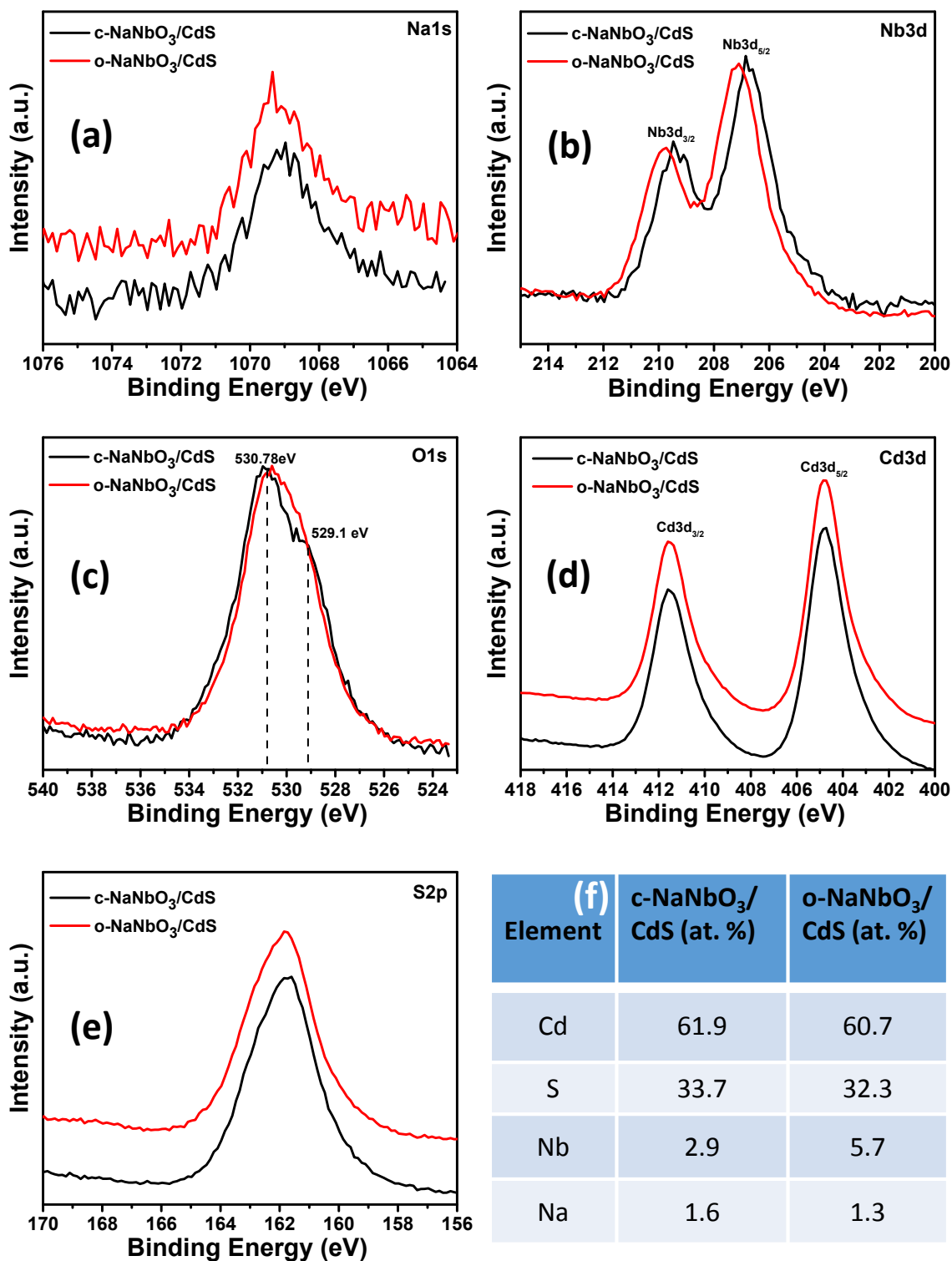
Figure S6. Na1s (a), Nb 3d (b), O1s (c) Cd3d (d) and S2p XPS lines of c-NaNbO$_3$/CdS cube and o-NaNbO$_3$/CdS cuboctahedron core/shell samples. The atomic percentage calculated for Cd, S, Nb and Na elements from the XPS data are shown in Table (f).

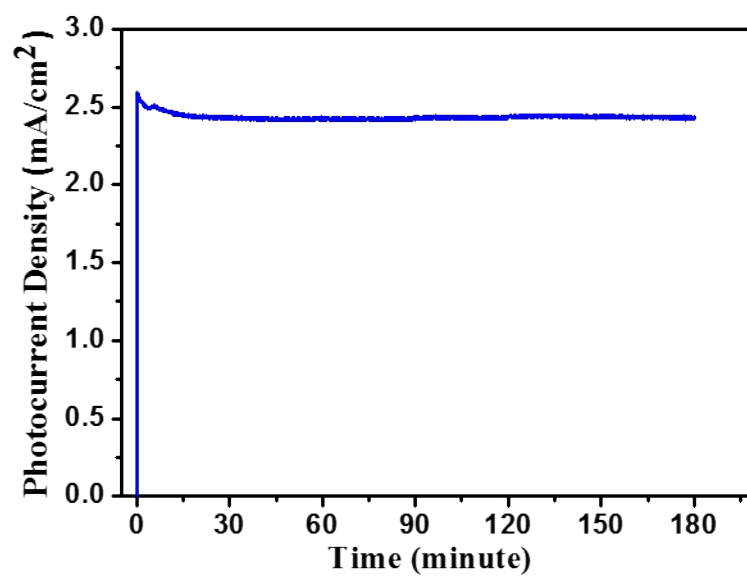| (f) Element	c-NaNbO$_3$/CdS (at. %)	o-NaNbO$_3$/CdS (at. %)
Cd	61.9	60.7
S	33.7	32.3
Nb	2.9	5.7
Na	1.6	1.3
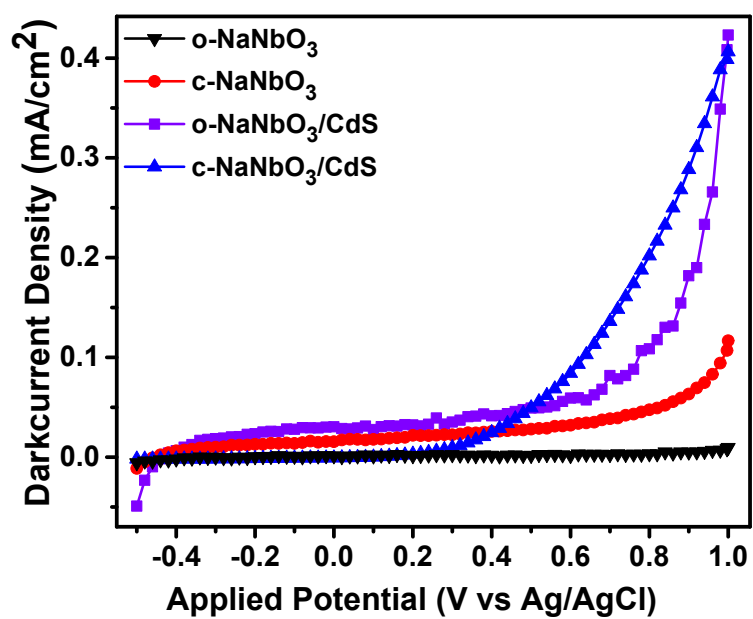
Figure S7. Current-voltage characteristics of all four samples under dark condition
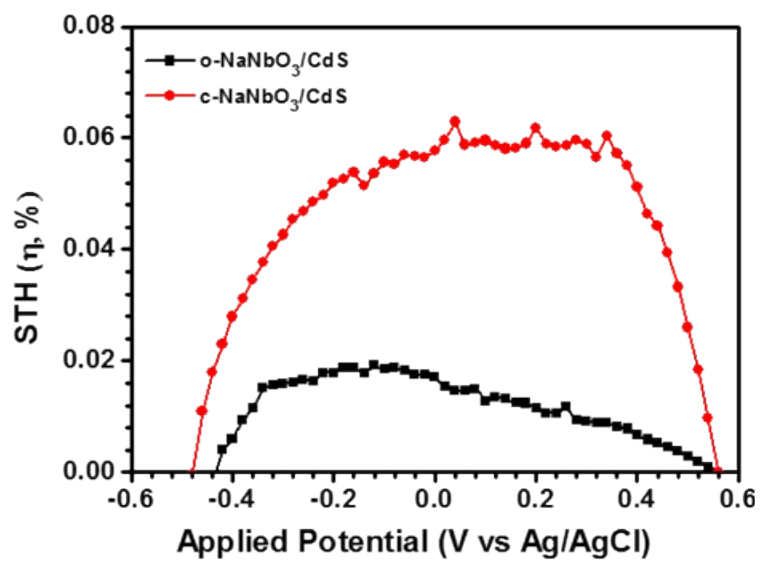
Figure S8. Solar-to-hydrogen (STH) conversion efficiencyof c-NaNbO$_3$/CdSand o-NaNbO$_3$/CdScore/shell in 0.5M Na$_2$SO$_4$ solution.

Figure S9. Current–time curves of c-NaNbO$_3$/CdS core/shell at 1.0 V versus Ag/AgCl under visible light illumination. A measurement was carried out in 0.5 M Na$_2$SO$_4$ solution.

Photodegradation efficiency plots of the prepared samples

The photodegradation efficiency curve (Figure S10) revealed that 98.5 % of the dye methylene blue[3] (MB) was degraded in the presence of c-NaNbO$_3$/CdS core/shell heterostructures, whereas around 86.4 %, 48.7 % and 1.2 % degradation was observed in the presence of o-NaNbO$_3$/CdS, CdS and NaNbO$_3$ respectively after 25 min. This degradation efficiency further revealed the higher catalytic activity of c-NaNbO$_3$/CdS cube than o-NaNbO$_3$/CdS core/shell due to higher surface energy of the facets involved in catalytic reaction.
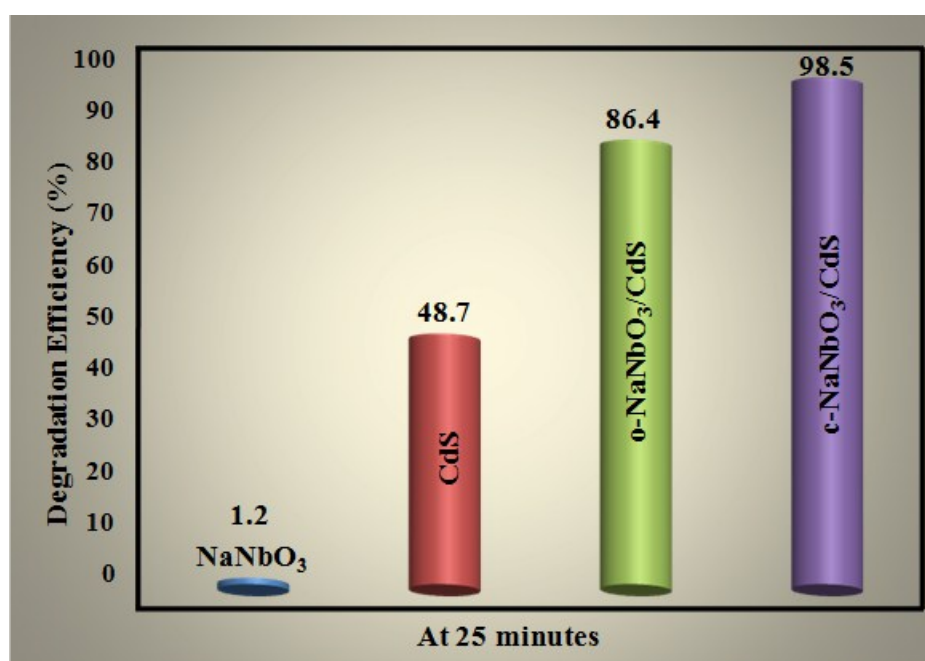
Figure S10. Degradation efficiency of NaNbO$_3$, CdS, c-NaNbO$_3$/CdS and o-NaNbO$_3$/CdS core/shell heterostructuresfor the degradation of MB dye aqueous solution under visible light irradiation.

Brunauer−Emmett−Teller (BET) surface area curves of the core/shell heterostructures

Nitrogen adsorption-desorption isotherms at ~77 K were measured after the samples were degassed in vacuum at ~70 °C for 6 h to remove unnecessary adsorbents from the surface of the as-synthesized samples (Figure S11). The BET measurements give a surface area value of about 16.18, 24.61 and 8.4 m^2g^{-1} for the barec-$NaNbO_3$ cube,o-$NaNbO_3$ cuboctahedron and CdS nanoparticles respectively whereas in the core/shell heterostructures highly enhanced surface area was recorded i.e. 86.12 m^2g^{-1} for c-$NaNbO_3$/CdS and 78.5 m^2g^{-1} for o-$NaNbO_3$/CdS core/shell. Enhanced surface area stemming from the rough surface of core/shell heterostructures facilitates more surface active sites, and thus we find that these $NaNbO_3$/CdS core/shell heterostructures are conducive to enhancing the photocatalytic and photoelectrochemical performance. The results of BET surface area analysis reveal that the growth of CdS shell onto the $NaNbO_3$cubes and cuboctahedra greatly enhances the surface area of the resulting core/shell heterostructures.
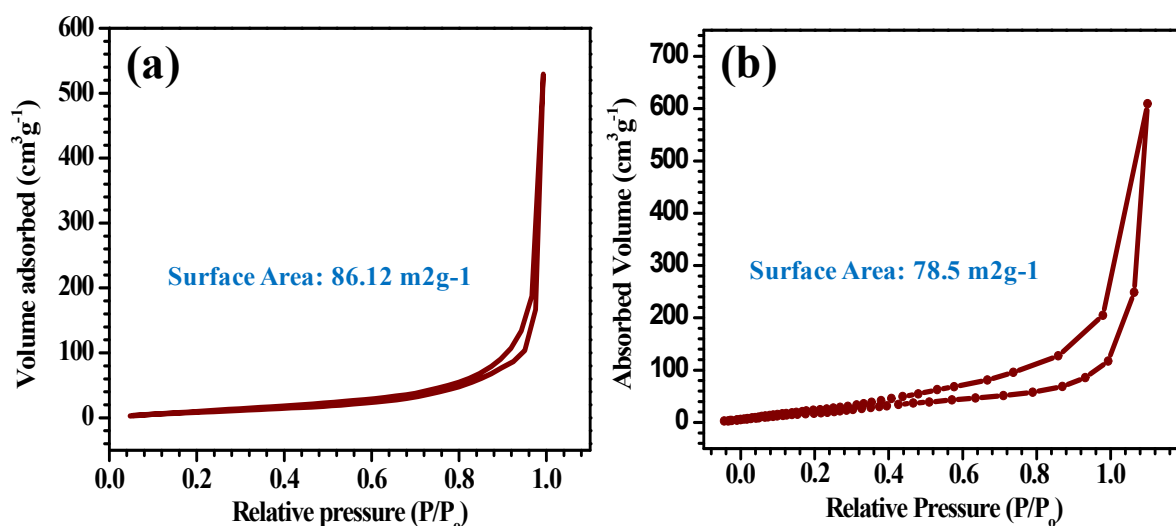

Figure S11. Brunauer−Emmett−Teller (BET) Nitrogen adsorption-desorption isotherms of (a) c-$NaNbO_3$/CdS cube and (b) o-$NaNbO_3$/CdS cuboctahedron core/shell heterostructures.

Study of the role of active species using different scavengers

The general mechanism of photocatalytic activity is quite well-understood. Under the irradiation of visible light, with photon energy equal to or exceeding the band gap of the semiconducting materials, the photogenerated charge carriers, namely the electrons and holes are generated. These electrons and holes perform the reduction and oxidation reactions to produce active oxygen radical species, such as superoxide radical anion ($O_2^{\bullet-}$) and hydroxyl radicals ($OH^{\bullet}$), which then participate in photocatalytic degradation of organic pollutants in water. Therefore, multiple controlled experiments utilizing various radical scavengers have been carried out in order to deeply understand the role of active oxygen species involved in the photodegradation of MB deploying c-NaNbO$_3$/CdS core/shell heterostructures. Separation of electrons and holes is always identified to be the essential step in the photocatalytic degradation.

To understand the role of photogenerated electrons in photocatalytic dye degradation, control experiments with and without the addition of AgNO$_3$ as an electron scavenger were carried out. As shown in Figure S12, the photocatalysis of MB over c-NaNbO$_3$/CdS core/shell heterostructures was incredibly retarded by 90.5% when AgNO$_3$ was injected into the reaction system. This result indicates the crucial role of photogenerated electrons in driving the photocatalytic degradation of MB. To clarify the role of photogenerated holes, ammonium oxalate (AO), a quencher for holes, was added in the MB solution. The reduction in photocatalytic efficiency of MB degradation from 98.5 to 93.4% indicates the insignificant role of holes either acting as the oxidizing agent or the originator of $OH^{\bullet}$ radicals in the MB degradation. We have also explored the role of $OH^{\bullet}$ and $O_2^{\bullet-}$ in the MB degradation, benzoquinone (BQ), used as a scavenger for $O_2^{\bullet-}$ and t-BuOH, an efficient $OH^{\bullet}$ quencher. A decline in photocatalytic efficiency from 98.5 to 8% was observed in BQ case and from 98.5 to 9% in t-BuOH. These above results clearly indicated the crucial roles played in dye degradation by electron, $OH^{\bullet}$ and $O_2^{\bullet-}$.
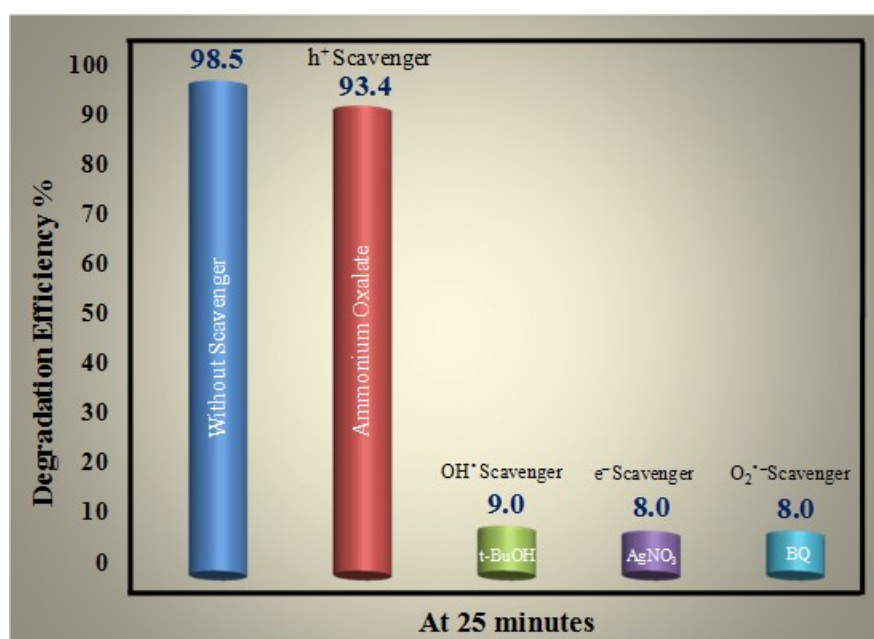
Figure S12. Controlled experiments performed using different active speciesscavengers for the photodegradation of MB over c-NaNbO$_3$/CdS core/shell heterostructures under illumination of visible light for 25 min.

Reusability experiment of the c-NaNbO₃/CdS core/shell heterostructures photocatalyst

We have performed a recyclability test, which is a determinative factor for a photocatalyst to be of viable utilization in environmental applications. To assess the recyclability performance of c-NaNbO₃/CdS core/shell heterostructures, we carried out five cycles of photocatalytic degradation of MB under illumination of visible light (Figure S13). The photocatalytic behaviour of c-NaNbO₃/CdS core/shell heterostructures exhibited almost no significant loss in photocatalytic activity after five cycles. Thus, this work has been an attempt to develop efficient, stable and better alternatives for photocatalytic applications. Our results unveil the superiority of c-NaNbO₃/CdS core/shell heterostructures over o-NaNbO₃/CdS core/shell heterostructures in photocatalytic performances.
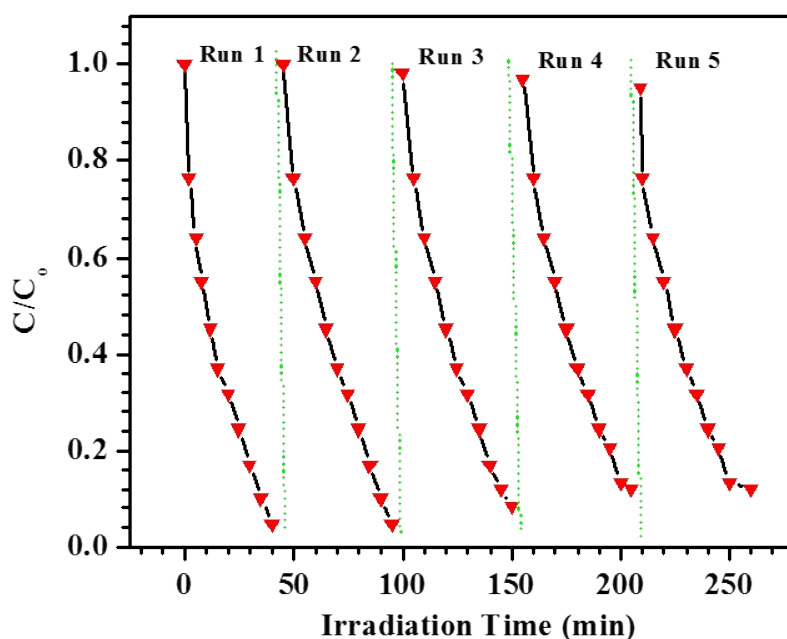
Figure S13. Reusability and stability test for degradation of MB during 5 cycles of dye photodegradation using c-NaNbO₃/CdS core/shell heterostructures in visible light irradiation.

References

(1) Compton, O. C.; Osterloh, F. E. Evolution of Size and Shape in the Colloidal Crystallization of Gold Nanoparticles. *J. Am. Chem. Soc*. **2007**, *129*, 7793-7798.

(2) Xu, C. S.; Cang, H.; Montiel, D.; Yang, H. Rapid and Quantitative Sizing of Nanoparticles using Three-Dimensional Single-ParticleTracking. *J. Phys. Chem. C,* **2007,** *111,* 32-35.

(3) Quinn, M. D. J.; Ho, N. H.; Notley, S. M. Aqueous Dispersions of Exfoliated Molybdenum Disulfide for use inVisible-Light Photocatalysis. *ACS Appl. Mater. Interfaces,* **2013**, *5*, 12751−12756.